Bioinorganic Chemistry

DOI: 10.1002/anie.200806056

Conformational Tuning of Magnetic Interactions in Metal–DNA Complexes**

*Sairam S. Mallajosyula and Swapan K. Pati**

One of the goals of nanotechnology is to achieve the controlled alignment and self-assembly of atoms and molecules at the atomic scale.[1] Owing to the efficient self-assembly properties of DNA, it shows promise as an efficient structural scaffold for the self-assembly of complex nanostructures in a highly controlled fashion.[2] Synthetic chemists have explored the possibility of replacing naturally occurring bases by alternative bases of different functionalities to allow the modification of DNA in a highly specific and site-selective manner.[3] Recent experimental studies have shown that upon replacement of hydrogen-bonded base pairing by metal-mediated base pairing in DNA, it is possible to align metal ions within the double helical DNA scaffold, leading to the formation of metal–DNA (M-DNA) complexes.[4]

Using a hydroxypyridone–metal base pair (H-MBP) (Supporting Information, Figure S1a), Tanaka et al. reported the alignment of up to five Cu^{2+} ions within the DNA scaffold.[5] Electron paramagnetic resonance (EPR) studies showed that the Cu^{2+} centers were ferromagnetically coupled to one another, with each Cu^{2+} center being in a distorted square-planar geometry. In an independent work, Clever and Carell reported the alignment of up to ten Cu^{2+} ions within the DNA double helix using a salicylaldehyde MBP (S-MBP) in the presence of an equimolar amount of ethylenediamine (en; Supporting Information, Figure S1b).[6] However, no magnetic measurements were made for the M-DNA with S-en-MBPs. In a collaborative effort, the two research groups were then able to align Cu^{2+} and Hg^{2+} ions within the same DNA scaffold, thereby achieving a mixed-metal–DNA adduct. The H-MBP and S-en-MBPs were used to align the Cu^{2+} ions, and the pyridine and thymine MBPs were used to align the Hg^{2+} ions.[7] The site-specific alignment of magnetic (Cu^{2+}; $3d^9$) and non-magnetic (Hg^{2+}; $5d^{10}$) ions at different positions in the same scaffold highlighted the potential of using these M-DNA systems as low-dimensional magnetic arrays.[8]

As very limited magnetic studies are available for these systems, the nature of their magnetic interactions remains debatable. A lack of crystallographic data also hinders an understanding of the magnetic interactions. In this regard, theoretical ab-initio calculations[9] can provide useful insights into understanding the magnetostructural properties of these systems, which in turn can be used to realize the advantages of controlled self-assembly of these structures. Herein, we report the first density-functional theory (DFT) calculations for the complete M-DNA system, inclusive of the DNA backbone and the end base pairs. We studied the alignment of up to four Cu^{2+} ions chelated by H-MBPs and S-en-MBPs within the DNA scaffold. From our calculations, we find that the nature of the magnetic interactions is strongly dependent on the conformational freedom of the MBPs.

We used the SIESTA package for our extensive first-principles DFT calculations.[10] The PBE version of the generalized gradient approximation (GGA) functional was adopted for exchange correlation.[11] A double-ζ basis set with the polarization orbitals was included for all the atoms,[12] and the semi-core 3p orbital was included in the valance orbitals for the copper atom. A real-space mesh cut-off of 300 Ry was used for all the calculations, which were carried out in supercells chosen such that the interactions between the neighboring fragments were negligible.[13] Atomic relaxations were performed until the forces on the atoms were not larger than 0.04 eV $Å^{-1}$. The DNA phosphate backbone was neutralized using a methyl phosphonate modification, which does not alter the structural stability of the DNA duplex structure.[14] These calculations are computationally very expensive owing to the dynamical fluctuations of the DNA backbone. Throughout, hydroxypyrido-incorporated DNA is denoted as *n*H-DNA, and bis(salicyclaldehyde)ethylenediamine-incorporated DNA as *n*S-(en)-DNA, where *n* corresponds to the number of Cu^{2+} ions aligned along the DNA scaffold.

We will first highlight the stability of the M-DNA systems. It was found that single-strand oligonucleotides with multiple MBP units did not form the duplex DNA structure in the absence of metal ions.[5–7] From melting-temperature (T_m) studies, it was found that the M-DNA duplexes were stable in comparison to their corresponding natural DNA duplexes.[4] Incorporation of a H-MBP increased the T_m by 13 K,[15] whereas an S-en-MBP increased the T_m by 40 K. In the absence of ethylenediamine, S-MBP also a showed comparable increase of T_m as H-MBP,[16] highlighting the stability of the S-en-MBP in the presence of the interlinking ethynenediamine unit.

To analyze the relative stability of the H-MBP and S-en-MBP, we calculated the energy required to displace the Cu^{2+} ion from the M-DNA scaffold. The displacement energy E_d is defined as:

[*] Dr. S. S. Mallajosyula, Prof. S. K. Pati
Theoretical Sciences Unit
Jawaharlal Nehru Centre for Advanced Scientific Research
Jakkur Campus, Bangalore 560 064 (India)
Fax: (+91) 80-2208-2766/2767
E-mail: pati@jnacsr.ac.in
Homepage: http://www.jncasr.ac.in/pati

[**] S.S.M. thanks CSIR for the SR fellowship. S.K.P. acknowledges CSIR and DST, Government of India, and AOARD, US Air Force, for research grants.

Supporting information for this article is available on the WWW under http://dx.doi.org/10.1002/anie.200806056.

$$E_d = \left[nE_{Cu(OH)_2} + E_{sca}\right] - \left[2nE_{H_2O} + E_{M-DNA}\right] \quad (1)$$

where $E_{Cu(OH)_2}$ is the energy of a $Cu(OH)_2$ molecule, E_{sca} is the energy of the M-DNA scaffold with the Cu^{2+} ions removed form the structure and the subsequent oxygen binding sites protonated to maintain charge neutrality, E_{H_2O} is the energy of a water molecule, E_{M-DNA} is the energy of the M-DNA structure, and n is the number of Cu^{2+} ions in the M-DNA structure. E_d for 1H-DNA and 1S-en-DNA is $+3.68$ eV ($+84.86$ kcal mol^{-1}) and $+3.58$ eV ($+82.55$ kcal mol^{-1}), respectively (the positive value indicates the stabilization of the M-DNA structure). For $n>1$, nS-en-DNA is stabilized over nH-DNA. To estimate E_d for $n>1$, we analyzed the displacement energy per Cu^{2+} ion for each system size (E_d/n); for nS-en-DNA systems we find that E_d/n converges to 3.36 eV, and E_d/n for nH-DNA shows an odd–even behavior (Supporting Information, Figure S1c). Note that owing to the presence of the strong metal coordinate bond in MBPs, the stabilization energy upon the formation of MBP (ca. 83 kcal mol^{-1}) is greater than the stabilization energy upon the formation of hydrogen-bonded base pairs, the scale of which varies between 9–25 kcal mol^{-1}.[17]

With an understanding of the stability of these M-DNA systems, we turned our attention to the structural aspects of these systems. Upon optimization of the geometries of 1H-DNA and 1S-en-DNA (Supporting Information, Figure S2a and S2b), we find that for both the structures, the Cu^{2+} ion is present in a distorted square-planar geometry, with the dihedral angle between the hydroxypyridone and salicylaldehyde units on the either side of Cu^{2+} ion in 1H-DNA and 1S-en-DNA being 13.83° (Figure 1a) and 8.85° (Figure 1b), respectively. This observation is in accordance with the EPR studies for 1H-DNA.[5] An analysis of the Cu–O(N) bond lengths and the O(N)-Cu-O(N) bond angles in H-MBP and S-en-MBP reveals the differences between the two MBPs (Supporting Information, Figure S3). H-MBP favors an asymmetric square-planar coordination with equivalent Cu–O bond lengths and inequivalent O-Cu-O bond angles (Figure 1a), the resultant configuration being similar to the open configuration observed in Watson–Crick base pairs.[18] On the other hand, S-en-MBP favors a symmetric square-planar coordination with nearly equivalent bond lengths and bond angles (Figure 1b). The symmetric coordination in S-en is a result of the interlinking of the two salicylaldehyde units by the ethylenediamine linker.

The optimized geometries of 2H-DNA and 2S-en-DNA are presented in Figure 1c and 1d, respectively. For 2H-DNA, the H-MBP are found to be present in a distorted square-planar arrangement, with the Cu–Cu distance being 3.22 Å, which is 0.53 Å less than the Cu-Cu distance in 2S-en-DNA (3.75 Å), for which the planes of the two S-en-MBP units are held nearly parallel to each other. On closer inspection, we find that this reduction in the Cu–Cu distance for 2H-DNA is due to the interplane Cu–O bonding interactions. In Figure 1e, we present the detailed structure of H-MBP from 2H-DNA. The oxygen atoms O(4a) and O(2b) belonging to the lower and upper H-MBPs interact with the Cu(b) and Cu(a) ions, respectively. These four atoms O(4a), O(2b), Cu(b), and Cu(a) form a distorted convex quadrangle with the Cu–O

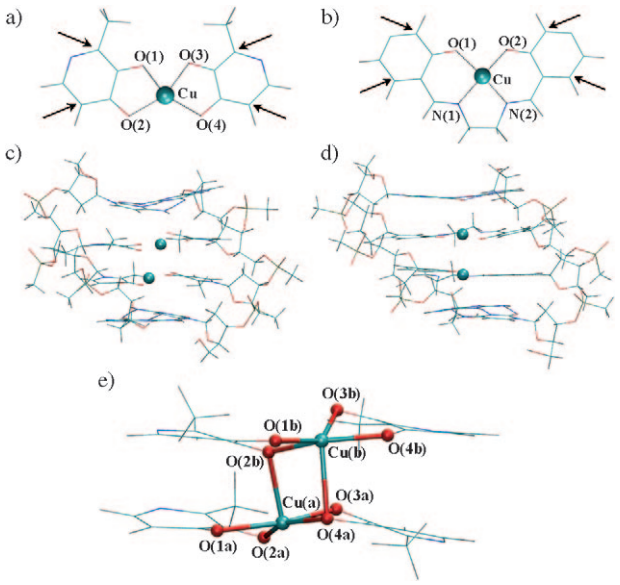

Figure 1. Optimized geometries of a) H-MBP, b) S-en-MBP, c) 2H-DNA, and d) 2S-en-DNA. Arrows indicate the atoms between which the dihedral angle is calculated (see text for details). e) Geometry of the H-MBP in 2H-DNA. Selected bond lengths [Å] and angles [°]: Cu(a)–O(4a) 2.14, O(4a)–Cu(b) 2.42, Cu(b)–O(2b) 2.02, O(2b)–Cu(a) 2.27; Cu(a)-O(4a)-Cu(b) 89.76, Cu(b)-O(2b)-Cu(a) 97.12.

bond lengths (and Cu-O-Cu angles) varying between 2.02 Å and 2.42 Å (89.76° and 97.12°). Thus, the independent conformational motion of the H-MBP in either DNA strands leads to formation of interplane Cu–O bonds, whereas the interlinking of the two salicylaldehyde units by the ethylenediamine linker in S-en-MBP leads to the parallel alignment of the two S-en-MBP in 2S-en-DNA.

In Figure 2a (see also the Supporting Information, Figure S4a), the optimized geometries of 4S-en-DNA (3S-en-DNA) are presented. The square-planar S-en-MBP units are aligned in an ordered pairwise-stacked geometry, with no out-of-plane Cu–O interactions. However, the H-MBPs in 3H-DNA (Supporting Information, Figure S4b) and 4H-DNA (Figure 2b) are in a distorted square-planar geometry, with interplane Cu–O bonding interactions. Each Cu^{2+} ion is coupled to its neighboring Cu^{2+} ion by two bridging oxygen

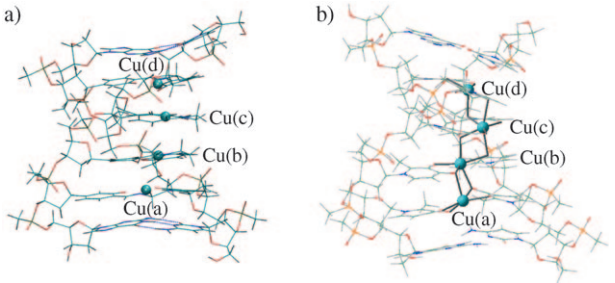

Figure 2. Optimized geometries of a) 4S-en-DNA (Cu(a)–Cu(b) 3.16, Cu(b)–Cu(c) 4.20, Cu(c)–Cu(d) 3.30 Å); and b) 4H-DNA (Cu(a)–Cu(b) 3.28, Cu(b)–Cu(c) 3.41, Cu(c)–Cu(d) 3.26 Å).

atoms, leading to the formation an extended Cu–O network (Supporting Information, Figure S5). The Cu–O bond lengths (and Cu-O-Cu bond angles) vary between 2.00 Å and 2.57 Å (94.11° and 111.12°) for 3H-DNA and 2.03 Å and 2.37 Å (92.84° and 109.74°) for 4H-DNA (Supporting Information, Table S1). Of note, in the four-atom convex quadrangle structure, the Cu-O-Cu bond angle associated with longer Cu–O bonds is closer to 90°, whereas the Cu-O-Cu bond angle associated with shorter Cu–O bonds is closer to 104°. The apparent differences between the *n*S-en-DNA and *n*H-DNA structures are thus clear: whereas both MBPs lead to the alignment of Cu^{2+} ions within the DNA scaffold, the alignment of the Cu^{2+} ions in *n*S-en-DNA is facilitated by the ordered pairwise stacking of the S-en-MBPs, whereas the same effect in *n*H-DNA is facilitated by the formation of the extended Cu–O network.

We then turned our attention to the magnetic exchange interactions in these systems. Specifically, we concentrated on the 2S-en-DNA and 2H-DNA systems to probe the stability of the corresponding highest spin (HS) and lowest spin (LS) states. The HS state is the state with all the spins aligned parallel to each other, and the LS state being the singlet (doublet) state for an even (odd) number of Cu^{2+} ions (see the Supporting Information for details of the broken-symmetry calculations). To estimate the relative stability of the spin states, we calculated the spin stabilization energy (ΔE_s) as the energy difference between the HS and LS spin states; that is, $\Delta E_s = E_{HS} - E_{LS}$. For 2S-en-DNA, the LS state is stabilized over the HS state by $\Delta E_s = +1.3$ meV, whereas for 2H-DNA, the HS state is stabilized over the LS state by $\Delta E_s = -4.2$ meV (the negative ΔE_s indicates the stabilization of the HS state). From the spin-density distribution corresponding to the LS and HS states for 2S-en-DNA and 2H-DNA (Supporting Information, Figure S6) we found that for both S-en-MBP and H-MBP, the spin density is delocalized over the Cu^{2+} ions and the chelating nitrogen and oxygen atoms, and that the spin ordering is not affected by the sugar/phosphate backbone. From the energies of the corresponding spin configurations, we obtained an estimate of the exchange coupling constant J, assuming Heisenberg spin–spin interactions ($H = -J\vec{S}_1\vec{S}_2$). For 2S-en-DNA, J is antiferromagnetic (AFM), with a magnitude of -1.3 meV ($-10.49\ cm^{-1}$); for 2H-DNA, J is ferromagnetic (FM) with a magnitude of 4.2 meV ($33.87\ cm^{-1}$).

The origins of the AFM and FM coupling in 2S-en-DNA and 2H-DNA can be traced back to the structural differences between the two systems, and can be explained in the light of the Goodenough–Kanamori rules and the orthogonality of the magnetic orbitals.[19,20] In 2S-en-DNA, because of the ordered pairwise-stacked arrangement of the S-en-MBPs, no strong coupling exists between the two Cu^{2+} ions, leading to an AFM coupling. Such a cation–cation direct exchange process leading to weak AFM coupling is in accordance with the Goodenough–Kanamori rules.[19] It is to be noted that the magnitude of such an exchange coupling is very sensitive to the cation–cation separation, which is more apparent for 3S-en-DNA and 4S-en-DNA.

To understand the origins of the FM coupling in 2H-DNA requires the principle of orthogonality of the magnetic orbitals.[20] According to the Heitler–London model, the exchange coupling constant can be expressed as $J = K + 2\beta S_{ovl}$, where K is the two-electron exchange integral, which is positive, and β is the resonance coupling (negative) and S_{ovl} is the overlap integral. Thus, J can be effectively expressed as $J = J_{FM} + J_{AFM}$. The latter term (J_{AFM}) vanishes when the two magnetic orbitals are orthogonal to each other (i.e., $S_{ovl} = 0$), leading to FM exchange coupling. Therefore, we analyzed the highest-occupied molecular orbitals of 2H-DNA. In Figure 3,

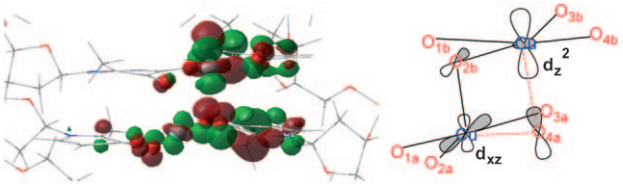

Figure 3. The SOMO orbital of 2H-DNA. The Cu-O-Cu-O quadrangle is shown in the ball and stick model and the rest of the DNA structure is shown in the wireframe model (left). For clarity, only atoms that contribute to the orbital density are shown (see the Supporting Information, Figure S8, for the complete DNA backbone). The right-hand image shows a sketch of the magnetic orbitals, dashed lines highlight the orthogonality of the orbitals.

the SOMO (singly occupied molecular orbital) of 2H-DNA is presented (see the Supporting Information, Figure S7, for the orbital plot of the degenerate SOMO−1). The orbitals are well-localized on Cu^{2+} and the chelating oxygen atoms. Note that for the SOMO, the magnetic orbital has a d_{xz} symmetry at Cu(a) and d_{x^2} symmetry at Cu(b). Thus, from the symmetry characteristics of the magnetic orbitals, it can be seen that the orbital contributions from the two Cu^{2+} centers are orthogonal to each other, leading to FM coupling. Interestingly, such FM exchange coupling has been observed earlier for hydroxo- and alkoxo-bridged Cu^{II} binuclear complexes $\{Cu_2O_2\}$,[21] in which the exchange coupling was found to be dependent on the Cu–Cu distance, Cu-O-Cu bond angle, and the hinge distortion of the bridge. For various $\{Cu_2O_2\}$ systems, the FM exchange coupling J was found to vary from $172\ cm^{-1}$ to $12\ cm^{-1}$; the Cu–Cu distance and Cu-O-Cu bond angle ranged from 2.847 Å to 2.914 Å and 95.6° to 97°, respectively.[22] However, for the 2H-DNA presented herein, the FM exchange coupling J is $33.87\ cm^{-1}$ for a Cu–Cu distance of 3.22 Å and Cu-O-Cu bond angles of 89.76° and 97.12°. Note that there are differences between the Cu-O-Cu network studied herein and the earlier studies, which mainly arise because of the symmetry of the intervening orbitals involved in the exchange pathway.[21,22] The main feature is that the near orthogonality of the intervening magnetic orbitals is brought about by the formation of the four-atom $\{Cu_2O_2\}$ convex quadrangle structure in the 2H-DNA herein by out-of-plane Cu–O interactions.

The ΔE_s for 3S-en-DNA and 4S-en-DNA is less than 0.1 meV, which is due to the large cation–cation separation distances, as already mentioned. Thus, neither of the spin states is preferred over the other, thereby leading to a paramagnetic arrangement of the spins in 3S-en-DNA and 4S-en-DNA. On the other hand, ΔE_s for 3H-DNA and 4H-DNA

are −12.01 meV and −28.53 meV, respectively. Using the calculated ΔE_s values and assuming Heisenberg spin–spin interactions, the FM exchange coupling J for 3H-DNA and 4H-DNA are found to be 64.60 cm^{-1} and 97.29 cm^{-1}, respectively (see the Supporting Information for calculation details). Thus, the HS state is highly stabilized over the LS state, with the stabilization energy and FM exchange coupling increasing with the system size.

To probe whether the spin–spin interactions can effect transport behavior, we calculated the optical conductivity for the *n*S-en-DNA and *n*H-DNA systems. The optical conductivity is given by the Kubo formula:

$$\sigma_{1,\mu}(\omega) = \pi \frac{e^2}{V} \frac{1 - e^{-\beta\hbar\omega}}{\omega} \sum_{n,m} \frac{e^{-\beta\varepsilon_n}}{Z} \delta(\varepsilon_n - \varepsilon_m - \hbar\omega) \left|\langle n|j_\mu|m\rangle\right|^2 \qquad (2)$$

where ε_n and $|n\rangle$are the energies and eigenstates of the DFT Hamiltonian. V denotes the volume of the unit cell and j_μ is the μth component of current. The conductivity computed herein does not include time-dependent DFT or scissors corrections. The conductivity, which is dependent on the frequency ω, is calculated along the strand direction.

Nonzero contributions to the optical conductivity for natural DNA appear only above the π–π* transition (>3 eV).[23] Thus, any strong low-lying excitations for the M-DNA systems below 2 eV in the optical conductivity profile can be probed for the signature of spin–spin coupling.

The low-frequency optical conductivity of *n*S-en-DNA (n = 1–4) is presented in Figure 4a. For all the *n*S-en-DNA systems, we observe a strong peak in the optical conductivity profile centered around 1.78 eV, with a corresponding shoulder centered at 1.62 eV. There are no strong peaks in the optical conductivity spectrum below 1.5 eV. The intensity of the peak at 1.78 eV is strengthened with increasing system size, clearly indicating the non-interacting and thus the additive nature of S-en-MBP in the *n*S-en-DNA scaffold.

The low-frequency optical conductivity of *n*H-DNA (n = 1–4) is shown in Figure 4b. For 1H-DNA, the low-frequency excitation has two strong peaks centered at 0.79 eV and 1.76 eV, which are split into five peaks centered at 0.67 eV, 0.92 eV, 1.31 eV, 1.62 eV and 1.73 eV for 2H-DNA. Interestingly, these peaks undergo further splitting on addition of subsequent H-MBP. Of note is the appearance of strong low-frequency excitations at 0.61 eV and 0.30 eV for 3H-DNA and 4H-DNA, respectively, which is a clear signature of increasing FM spin–spin coupling strengths in the *n*H-DNA systems.

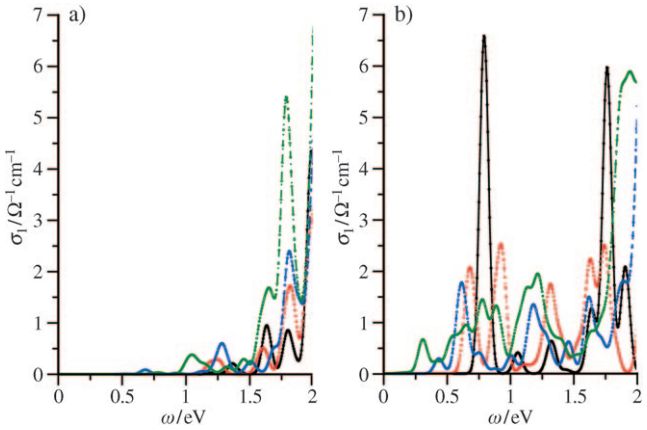

Figure 4. Low-frequency region of optical conductivity for a) *n*S-en-DNA and b) *n*H-DNA (n = 1–4). The theoretical line spectra are broadened with Gaussian functions of width 0.05 eV. Legend: —— n = 1, ····· n = 2, – – – n = 3, –·–· n = 4.

It should be emphasized that optical conductivity could be used as a soft-probe technique for distinguishing between these two M-DNA scaffolds. The optical conductivity profile shows linear scaling for the *n*S-en-DNA system, while the appearance of new peaks and shifting of the peaks with addition of monomers serves as an indicator for identifying spin–spin interactions in the *n*H-DNA systems. Therefore, the mere incorporation of magnetic ions into the DNA architecture does not lead to FM coupling between the magnetic centers. The formation of the four-atom $\{Cu_2O_2\}$ convex-quadrangle structure arising from out-of-plane Cu–O bonding interactions is crucial for the realization of FM coupling between the Cu^{2+} centers, as it ensures the orthogonality of the magnetic orbitals. On the other hand, the interlinking of the two salicylaldehyde units by the ethylenediamine linker in S-en-MBP leads to an ordered pairwise-stacked arrangement of the S-en-MBPs in *n*S-en-DNA, which suppresses magnetic coupling.

Before concluding, we comment on the selective multiple-ion (Cu^{2+}, Hg^{2+}) assembly within the DNA scaffold.[7] The optimized geometry of H-thymine-H DNA shows that H-MBP chelates the Cu^{2+} ions, whereas the thymine MBP chelates the Hg^{2+} ion (Supporting Information, Figure S9). This arrangement leads to the separation of the magnetic ions by a non-magnetic species. For this system, ΔE_s is less than 0.1 meV, thereby leading to a paramagnetic arrangement of the spins. It should be stressed that with a controlled insertion of thymine MBP among H-MBP domains, it is possible to create magnetic domains within the DNA scaffold. Creation of such domains can then be used as qubits for quantum computing and data storage devices.

In conclusion, we have shown that the magnetic interactions in the M-DNA structures are strongly dependent on the conformational characteristics of the MBP. The formation of an extended Cu–O network in *n*H-DNA favors FM coupling, whereas the ordered pairwise-stacked arrangement in *n*S-en-DNA suppresses magnetic coupling. Optical conductivity can be used as a soft-probe technique for distinguishing between the two DNA structures. These M-DNA systems show potential as low-dimensional magnetic arrays for advanced device applications, such as qubits.

Received: December 12, 2008
Revised: March 10, 2009
Published online: May 26, 2009

Keywords: DNA structures · metalated base pairs · metal–metal interactions · nanotechnology

[1] J.-M. Lehn, *Supramolecular Chemistry*, Wiley-VCH, Weinheim, **1995**.
[2] a) N. C. Seeman, *Angew. Chem.* **1998**, *110*, 3408–3428; *Angew. Chem. Int. Ed.* **1998**, *37*, 3220–3238; b) C. A. Mirkin, R. L.

Letsinger, R. C. Mucic, J. J. Storhoff, *Nature* **1996**, *382*, 607 – 609; c) A. P. Alivisatos, K. P. Johnsson, X. G. Peng, T. E. Wilson, C. J. Loweth, M. P. Bruchez, P. G. Schultz, *Nature* **1996**, *382*, 609 – 611.
[3] E. T. Kool, *Acc. Chem. Res.* **2002**, *35*, 936 – 943.
[4] a) G. H. Clever, C. Kaul, T. Carell, *Angew. Chem.* **2007**, *119*, 6340 – 6350; *Angew. Chem. Int. Ed.* **2007**, *46*, 6226 – 6236; b) K. Tanaka, M. Shionoya, *Coord. Chem. Rev.* **2007**, *251*, 2732 – 2742; c) H.-A. Wagenknecht, *Angew. Chem.* **2003**, *115*, 3322 – 3324; *Angew. Chem. Int. Ed.* **2003**, *42*, 3204 – 3206.
[5] K. Tanaka, A. Tengeiji, T. Kato, N. Toyama, M. Shionoya, *Science* **2003**, *299*, 1212 – 1213.
[6] G. H. Clever, T. Carell, *Angew. Chem.* **2007**, *119*, 254 – 257; *Angew. Chem. Int. Ed.* **2007**, *46*, 250 – 253.
[7] K. Tanaka, G. H. Clever, Y. Takezawa, Y. Yamada, C. Kaul, M. Shionoya, T. Carell, *Nat. Nanotechnol.* **2006**, *1*, 190 – 194.
[8] J. Müller, *Nature* **2006**, *444*, 698.
[9] a) S. S. Mallajosyula, S. K. Pati, *Phys. Rev. Lett.* **2007**, *98*, 136601 – 136604; b) H. Zhang, A. Calzolari, R. Di Felice, *J. Phys. Chem. B* **2005**, *109*, 15345 – 15348.
[10] J. M. Soler, E. Artacho, J. D. Gale, A. Garcia, J. Junquera, P. Ordejón, D. Sánchez-Portal, *J. Phys. Condens. Matter* **2002**, *14*, 2745 – 2779.
[11] J. P. Perdew, K. Burke, M. Ernzerhof, *Phys. Rev. Lett.* **1996**, *77*, 3865 – 3868.
[12] O. F. Sankey, D. J. Niklewski, *Phys. Rev. B* **1989**, *40*, 3979 – 3995.
[13] Super-cell sizes: a) 1H-DNA, 1S-(en)-DNA: $35 \times 35 \times 35$ Å^3; b) 2H-DNA, 2S-(en)-DNA: $40 \times 40 \times 40$ Å^3; c) 3H-DNA, 3S-(en)-DNA: $45 \times 45 \times 45$ Å^3; d) 4H-DNA, 4S-(en)-DNA: $50 \times 50 \times 50$ Å^3.
[14] a) D. Hamelberg, L. D. Williams, W. D. Wilson, *Nucleic Acids Res.* **2002**, *30*, 3615 – 3623; b) S. S. Mallajosyula, S. K. Pati, *J. Phys. Chem. B* **2007**, *111*, 13877 – 13880.
[15] K. Tanaka, A. Tengeiji, T. Kato, N. Toyama, M. Shiro, M. Shionoya, *J. Am. Chem. Soc.* **2002**, *124*, 12494 – 12498.
[16] G. H. Clever, K. Polborn, T. Carell, *Angew. Chem.* **2005**, *117*, 7370 – 7374; *Angew. Chem. Int. Ed.* **2005**, *44*, 7204 – 7208.
[17] a) J. Sponer, J. Leszczynski, P. Hobza, *J. Phy. Chem.* **1996**, *100*, 1965 – 1974; b) S. S. Mallajosyula, A. Datta, S. K. Pati, *Synth. Met.* **2005**, *155*, 398 – 401.
[18] W. K. Olson, M. Bansal, S. K. Burley, R. E. Dickerson, M. Gerstein, S. C. Harvey, U. Heinemann, X.-J. Lu, S. Neidle, Z. Shakked, H. Sklenar, M. Suzuki, C.-S. Tung, E. Westhof, C. Wolberger, H. M. Berman, *J. Mol. Biol.* **2001**, *313*, 229 – 237.
[19] Goodenough, J. B. *Magnetism and the Chemical Bond*, VCH, New York, **1963**.
[20] O. Kahn, *Molecular Magnetism*, VCH, New York, **1993**.
[21] a) E. Ruiz, P. Alemany, S. Alvarez, J. Cano, *J. Am. Chem. Soc.* **1997**, *119*, 1297 – 1303; b) E. Ruiz, P. Alemany, S. Alvarez, J. Cano, *Inorg. Chem.* **1997**, *36*, 3683 – 3688.
[22] a) R. J. Majeste, E. A. Meyers, *J. Phys. Chem.* **1970**, *74*, 3497 – 3500; b) V. H. Crawford, H. W. Richardson, J. R. Wasson, D. J. Hodgson, W. E. Hatfield, *Inorg. Chem.* **1976**, *15*, 2107 – 2110; c) M. J. Katz, C. J. Shorrock, R. J. Batchelor, D. B. Leznoff, *Inorg. Chem.* **2006**, *45*, 1757 – 1765; d) I. Castro, J. Faus, M. Julve, M. Verdaguer, A. Monge, E. Gutierrez-Puebla, *Inorg. Chim. Acta* **1990**, *170*, 251 – 257; e) J. Sletten, A. Soerensen, M. Julve, Y. Journaux, *Inorg. Chem.* **1990**, *29*, 5054 – 5058.
[23] A. Hübsch, R. G. Endres, D. L. Cox, R. R. P. Singh, *Phys. Rev. Lett.* **2005**, *94*, 178102.

